Pressure observations by the Curiosity rover: Initial results

A.-M. Harri,[1] M. Genzer,[1] O. Kemppinen,[1] H. Kahanpää,[1] J. Gomez-Elvira,[2] J. A. Rodriguez-Manfredi,[2] R. Haberle,[3] J. Polkko,[1] W. Schmidt,[1] H. Savijärvi,[1] J. Kauhanen,[1] E. Atlaskin,[1] M. Richardson,[4] T. Siili,[1] M. Paton,[1] M. de la Torre Juarez,[5] C. Newman,[4] S. Rafkin,[6] M. T. Lemmon,[7] M. Mischna,[5] S. Merikallio,[1] H. Haukka,[1] J. Martin-Torres,[2] M.-P. Zorzano,[2] V. Peinado,[2] R. Urqui,[2] A. Lapinette,[2] A. Scodary,[4] T. Mäkinen,[1] L. Vazquez,[8] N. Rennó,[9] and the REMS/MSL Science Team

Received 16 May 2013; revised 26 November 2013; accepted 3 December 2013; published 22 January 2014.

[1] REMS-P, the pressure measurement subsystem of the Mars Science Laboratory (MSL) Rover Environmental Measurement Station (REMS), is performing accurate observations of the Martian atmospheric surface pressure. It has demonstrated high data quality and good temporal coverage, carrying out the first in situ pressure observations in the Martian equatorial regions. We describe the REMS-P initial results by MSL mission sol 100 including the instrument performance and data quality and illustrate some initial interpretations of the observed features. The observations show both expected and new phenomena at various spatial and temporal scales, e.g., the gradually increasing pressure due to the advancing Martian season signals from the diurnal tides as well as various local atmospheric phenomena and thermal vortices. Among the unexpected new phenomena discovered in the pressure data are a small regular pressure drop at every sol and pressure oscillations occurring in the early evening. We look forward to continued high-quality observations by REMS-P, extending the data set to reveal characteristics of seasonal variations and improved insights into regional and local phenomena.

Citation: Harri, A.-M., et al. (2014), Pressure observations by the Curiosity rover: Initial results, *J. Geophys. Res. Planets*, *119*, 82–92, doi:10.1002/2013JE004423.

1. Introduction

[2] The Martian atmosphere has been observed by ground-based optical observations since the early 19th century [*Martin et al.*, 1992; *Zurek*, 1992]. Spacecraft observations started in the early to middle 1960s [e.g., *Kliore et al.*, 1965; *Snyder and Moroz*, 1992]. Observations have been accompanied and supplemented by increasingly sophisticated and varied modeling efforts in a range of spatial and temporal scales since late 1960s [e.g., *Leovy and Mintz*, 1969; *Pollack et al.*, 1990, 1993; *Haberle et al.*, 1993; *Barnes et al.*, 1993; *Forget et al.*, 1999; *Richardson et al.*, 2007]. Although our understanding of the Martian atmosphere and its processes is bound to be far less sophisticated and detailed than our understanding of the terrestrial atmosphere, the knowledge of the Martian atmospheric phenomena is probably second to no other planet in the solar system. Good overviews exist in the literature for the general circulation and climate [e.g., *Tillman et al.*, 1979; *Zurek et al.*, 1992; *Haberle et al.*, 1993; *Forget et al.*, 1999; *Richardson et al.*, 2007], regional and mesoscale phenomena [e.g., *Rafkin et al.*, 2001; *Spiga*, 2011], and the boundary layer [*Petrosyan et al.*, 2011].

[3] Surface pressure of the atmosphere has been estimated using remote sensing methods, both ground based [*Martin et al.*, 1992] and from spacecraft starting from Mariner 4 [*Kliore et al.*, 1965]. In situ pressure observations in the Martian atmosphere have been carried out by five landers. Further details are given in Table 1.

[4] The earlier pressure observations have shown that the surface pressure on Mars exhibits variations in several time scales and amplitudes. Shortest variations (few tens of seconds) are usually associated with thermal vortices (called "dust devils", if they carry an optically distinguishable dust load [*Zurek et al.*, 1992]). Thermal tides cause clearly detectable diurnal pressure variations especially at low latitudes, in relative terms much larger than in Earth's atmosphere. The traveling low- and high-pressure systems cause pressure variations in a 2–5 sols time range, especially

Additional supporting information may be found in the online version of this article.

[1]Finnish Meteorological Institute, Helsinki, Finland.
[2]Centro de Astrobiologia, Madrid, Spain.
[3]NASA AMES Research Center, San Francisco, California, USA.
[4]Ashima Research Inc., Pasadena, California, USA.
[5]NASA Jet Propulsion Laboratory, Pasadena, California, USA.
[6]Southwest Research Institute, Boulder, Colorado, USA.
[7]Texas A&M University, College Station, Texas, USA.
[8]University of Complutense, Madrid, Spain.
[9]University of Michigan, Ann Arbor, Michigan, USA.

Corresponding author: A.-M. Harri, Division of Earth Observation, Finnish Meteorological Institute, Helsinki, FI-00101 Finland. (Ari-Matti.Harri@fmi.fi)

2169-9097/14/10.1002/2013JE004423

Table 1. Summary of In Situ Pressure Observations and Observation Systems in the Martian Atmosphere

Lander	Sensor Type	Reference	Location	Duration	Platform
Viking Lander 1	magnetic reluctance diaphragm	*Hess et al.* [1977]	North subtropics	Martian years	stationary
Viking Lander 2	magnetic reluctance diaphragm	*Hess et al.* [1977]	North midlatitudes	Martian years	stationary
Mars Pathfinder	magnetic reluctance diaphragm	*Seiff et al.* [1997]	North subtropics	tens of sols	stationary
Phoenix	capacitive	*Taylor et al.* [2010]	North polar regions	tens of sols	stationary
MSL	capacitive	*Gómez-Elvira et al.* [2012]	equatorial regions	> 100 sols	mobile

in wintertime extratropics. In seasonal-to-annual time scales the CO_2 condensation-sublimation cycle at the polar regions gives rise to a seasonal variation of the order of 25 % in local surface pressure [*James et al.*, 1992].

[5] The Mars Science Laboratory (MSL) was targeted to the Gale Crater, a 154 km diameter formation located in the NE portion of the Aeolis quadrangle, on the boundary between the southern cratered highlands and the lowlands of Elysium Planitia [*Wray*, 2013]. The crater's central peak, Mount Sharp, rises about 5.5 km above the floor of the crater. MSL landed on 6 August 2012, onto the crater floor NW of Mount Sharp, at 4.6°S, at 137.4°E, and at 4.5 km below the datum. The landing season was few sols after the middle of the southern winter at areocentric longitude of $L_s \approx 151°$ [*Wray*, 2013].

[6] The Rover Environmental Monitoring Station (REMS) [*Gómez-Elvira et al.*, 2012] is part of the MSL scientific payload. REMS comprises instrumentation for the observation of atmospheric surface pressure (p_s), air and ground temperature (T, T_g), wind speed and direction ($\vec{V}$), relative humidity (H), and UV radiation. The station is designed for operations lasting at least a full Martian year. The pressure measurement subsystem of the REMS (REMS-P) is provided by the Finnish Meteorological Institute (FMI). REMS-P was successfully checked out in the first few sols of the mission and has been making regular observations since the MSL sol 9.

[7] The landing site region, the anticipated long duration of the observations, and the mobility of the platform offer good opportunities for observing complicated meteorological phenomena associated with different spatial and temporal scales. Although some characteristics of the pressure (for instance, related to the large-scale circulation) are likely to become apparent only after observations covering a substantial fraction of the full seasonal cycle, some effects are expected to be visible already after shorter-duration observations. Examples include variations due to the diurnal temperature variation, effects of the terrain, some effects of the large-scale circulation, and transient pressure drops associated with thermal vortexes. The REMS-P observations will add to the body of observations on previously discovered phenomena and may provide new findings. Together with other MSL instruments, the observations can further improve our understanding of near-surface atmospheric processes as well as the past and present climate and habitability of Mars.

[8] The structure of this paper is as follows: Section 2 describes the technology, operation, calibration, and

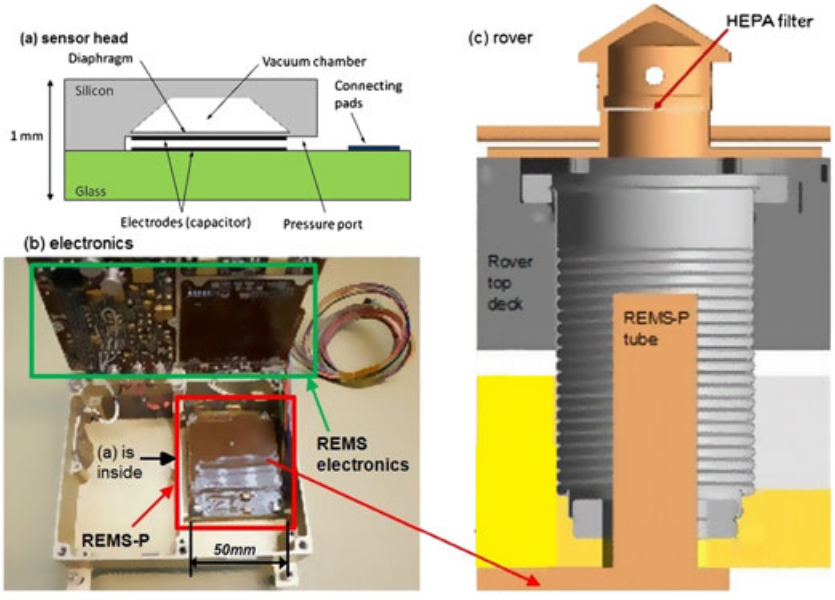

Figure 1. (a) The Barocap® is a silicon micromachined miniaturized capacitive sensor head. The measured pressure is fed between the two capacitor plates through an inlet port. Varying pressure bends the thin silicon membrane. One of the capacitor plates is attached to the bending silicon membrane generating varying capacitance. (b) REMS-P is accommodated inside the MSL rover body and embedded in the REMS electronics box, as shown on the left pane photo depicting the EM electronics. (c) The measured pressure is let in via a special inlet port on the deck of the MSL as shown on the right.

Table 2. Factors Limiting the REMS-P Performance[a]

Factor	LL	RSP2M	Notes
Warm-up time	150 s	1 s	
Noise	0.2 Pa	0.2 Pa	Peak to peak
Response time	1 s	1 s	
Shadow effect	1 Pa	1 Pa	Pressure drop
Repeatability variation	< 1.5 Pa	< 1.5 Pa	Peak to peak
Offset drift rate during cruise	+0.5 Pa/year	–3 to –5 Pa/year	
Estimated offset drift rate during mission	± 0.5 Pa/year	N/A	
Absolute uncertainty of single reading	< 2.7 Pa		MSL sols 0–100
Sampling interval	16 s	1 s	Nominal REMS observations strategy

[a]Columns LL and RSP2M give the characteristic measures of the factor for the LL and RSP2M sensor head types, respectively.

performance of the REMS-P system; section 3 describes the pressure observations made with REMS-P for MSL mission sols 1–100 and their initial analysis, whereas section 4 compares these observations with other missions' observations and with modeling results. Discussion, conclusions, and future prospects and plans are outlined in section 5. A companion paper [*Haberle et al.*, 2014] provides a more in-depth analysis of the pressure data and the phenomena they reveal. The companion paper emphasizes modeling and interpretation, whereas ours is focused on the pressure instrument performance and initial results.

2. REMS-P Implementation and Performance

2.1. REMS-P Overview

[9] The MSL pressure measurement instrument, REMS-P, provided by FMI is based on Barocap® sensor heads and associated Thermocap® sensor heads developed by Vaisala, Inc. REMS-P is located in the rover body, inside the REMS Instrument Control Unit (ICU), and is connected to the ambient atmosphere with a filter-protected measurement tube (Figure 1c). The total mass of REMS-P (including casing) is less than 40 g. Total operational power consumption is 15 mW.

[10] The Barocap® sensor head is a silicon micromachined device with the pressure-sensitive membrane made out of single-crystal silicon. The measurement is based on the distance of the capacitor plates (electrodes) changed by pressure, thus changing the capacitance of the sensor head. Two types of sensor heads are used in the REMS-P: The LL type has high stability but long warm-up time ($\simeq$ 150 s), while the RSP2M type is less stable but has a short warm-up time ($\simeq$ 1 s). The nominal capacitance of a Barocap® in Martian pressure is 10–15 pF depending on the sensor head type. The internal structure of a Barocap® sensor head is illustrated in Figure 1a.

[11] The Barocap® sensor heads have extensive flight heritage. Before REMS, they have been utilized in four Mars lander missions: Mars 96 [*Harri et al.*, 1998], Mars Polar Lander [*Paige et al.*, 1998], Beagle 2 [*Towner et al.*, 2004], and Phoenix [*Taylor et al.*, 2008, 2010] as well as in the Huygens/Cassini mission to the Saturnian moon Titan [*Harri et al*., 2006].

[12] REMS-P comprises of two transducer electronics sections placed on a single multilayer printed circuit board (dimensions 62 mm × 50 mm; Figure 1). REMS-P includes altogether four sensor heads, two in both transducers. Both transducers also include two Thermocap® housekeeping temperature sensors. Transducer 1 includes two RSP2M-type sensor heads, and transducer 2 one LL sensor head and one RSP2M-type sensor head. Transducer 2 is used for regular science measurements while transducer 1 is used only for so-called cross-calibration sessions (explained in the following chapter), carried out approximately every 100 sols.

2.2. Observational Strategy and Scheduling of REMS-P Measurements

[13] The REMS commissioning phase took place on MSL mission sols 2–8 and regular REMS (and REMS-P) observations started on sol 9 ($L_s \approx 155°$).

[14] The nominal observational strategy of the REMS instrument is to make observations for a period of 5 min each hour [*Gómez-Elvira et al.*, 2012]. During those periods, all REMS sensors (including the REMS-P) are measuring at the rate of one sample per second. However, within REMS-P only the RSP2M sensor head is read with 1 s intervals, the LL sensor head read interval is 16 s.

[15] REMS has also an extended mode, where data are acquired for longer time blocks, e.g., continuously for 1 h [*Gómez-Elvira et al.*, 2012]. The actual observation time allocated for REMS observations depends on availability of power, data volume, and many other issues dictated by MSL. During the first 100 sols, the cumulative observation time per sol of REMS was 2–10 h.

2.3. Calibration

[16] REMS-P was originally calibrated in April 2008 by FMI. After the rescheduling of the MSL launch, REMS-P was recalibrated in May 2009 [*Gómez-Elvira et al.*, 2012]. In these calibrations the output of REMS-P was measured at several pressure and temperature points under stable and changing temperature. The calibration temperature range was taken as the expected temperature range inside the REMS ICU during surface operations. In stable temperature calibrations, the temperature interval was 15°C; the pressure range was 0–1400 Pa (vacuum to Martian pressure range) with 100 Pa intervals. In the changing temperature calibrations, temperature was swept over the operational range down and up with rates ±15°C/h and ±30°C/h with pressure kept at constant 800 Pa. A Vaisala PTB201 pressure transmitter modified for the Martian pressure range was used as pressure reference. The accuracy of the reference sensor is 1 Pa, and its calibration is traceable to national standards.

[17] Based on results of environmental tests and experience from previous planetary missions, it was known that the

pressure dependence of Barocap® sensor heads is extremely stable but small changes in temperature dependence and offset may occur. In March 2011, after integration to the rover, calibration checks against FMI's reference sensor were performed to determine compensation parameters for changes in temperature dependence. Two calibration checks were performed during the interplanetary cruise using vacuum as reference. Readings measured in the second cruise checkout were used to compensate for the offset drift.

[18] After landing, all Barocap® sensor heads are periodically compared to each other and the high-stability LL-type sensor head to evaluate changes in their temperature dependence and offset that could have occurred during cruise and the landed mission. In this cross-calibration process hourly 5 min observations are performed during 1 sol such that the transducer 2 (containing the LL-type sensor head) is used for 4 min and the transducer 1 for 1 min. This is repeated approximately every 100 sols, the first two during sols 9–10 and sols 99–100. Based on these comparison measurements, the uncertainties caused by postlanding drift can be evaluated as explained in the following chapter. The prelanding drift for all sensors has been compensated using data acquired during interplanetary cruise.

2.4. Performance and Data Quality

[19] The preflight tests showed that REMS-P fulfilled all its performance requirements with clear margins. During the first 100 sols of the mission, REMS-P has worked flawlessly. However, there are sources of uncertainty that should be taken into account when using the data, depending predominantly on time scale. A compact overview of the REMS-P resolution, repeatability, and accuracy factors is given in Table 2 with more detailed descriptions of said factors below.

[20] In the time scale of seconds the *warm-up effect* plays a major role. It causes uncertainty in the readings of the LL sensor heads after power-up (in practice at the beginning of each observation session). This uncertainty decreases exponentially which is a sensor specific effect. The first 180 s (3 min) of LL sensor head measurements after each power-up are considered less reliable than the measurements thereafter. Thus, the readings from approximately the last 2 min of each 5 min session (instead of averages of the whole session) should be used in studies of phenomena with longer time scales. The RSP2M sensor heads are not affected by warm-up behavior so only they (and *not* LL sensor head readings) should be used when studying phenomena in time scales of seconds to minutes.

[21] *Noise* restricts the resolution of the sensor. The resolution of all Barocap® sensor heads, defined as the peak-to-peak value of noise, is ≈0.2 Pa. A peak noise of 0.2 Pa is good to detect most convective vortices; see e.g., the thorough exploration of Phoenix data by *Ellehoj et al.* [2010].

[22] The *response time* of the pressure sensor is ≈1 s according to test data. Thus, the response time has almost no effect on the data except that variations faster than the sampling interval are damped. Dust deposited on the filter during the mission could lengthen the response time. A test to study this will be performed using the REMS-P electrical model (EM). It is improbable that dust would have affected the response time during the first 100 sols of the mission taking into account the small amount of dust deposited on rover structures.

[23] Sometimes, small pressure drops (less than 1 Pa) occur when the REMS UV sensor is shadowed by rover structures. This *shadow effect* affects data measured around the beginning and end of UV-sensor shadowing. Because of this, the measurements taken in the time windows of –2 min to +3 min around both the start and the end of UV sensor shadowing are considered unreliable. The cause of this effect is not known. It might be caused by electrical interference between the two sensor systems.

[24] In the diurnal time scale the most important source of uncertainty is *repeatability variation* caused by the so-called slow temperature hysteresis [*Gómez-Elvira et al.*, 2012]. Variation in the sensor temperature causes artificial variation in the readings of all sensor head types. This effect affects the different sensor head types in different ways so diurnal pressure variations detected similarly by both LL and RSP2M sensor heads in transducer 2 cannot be the artifacts caused by this effect. Therefore, data from both sensor heads in transducer 2 should be used when studying diurnal pressure variations. During the mission, the diurnal variation in the sensor temperature has been similar as in one of the tests carried out after REMS-P integration to the rover. Therefore, we can estimate that the magnitude of the repeatability variation is of the same order than what was detected in the test, less than 1.5 Pa peak to peak. This estimate is supported by the observation that the difference between the readings of the two sensor heads in transducer 2 behaves in a similar way than in the test.

[25] In the seasonal time scale, the most important source of uncertainty is the offset *drift*. Aging affects slightly the offsets of the pressure readings of the sensor heads. The drift rate of the LL sensor head has been consistently circa +0.5 Pa/year (terrestrial year) throughout the calibrations, as well as during the interplanetary cruise phase. The drifts of the RSP2M sensor heads have been stronger and have varied more during calibrations. During cruise, all RSP2M sensor heads drifted in the opposite direction than the LL sensor head with rates –3 Pa/year to –5 Pa/year. However, during the first 100 sols, their drift compared both to LL and to each other was less than 0.4 Pa. This means that on Mars the drift has slowed down and so it is likely that the LL is not drifting more than it did during the cruise. But even with the same rate as during the cruise, the drift during 100 sols would be no more than 0.2 Pa for the LL sensor. As the LL sensor head is the most stable Barocap type, it is recommended that it be used when studying seasonal pressure variations.

[26] The REMS-P sensor head cross-calibrations have also revealed that the temperature dependence of the sensor heads did not drift compared to each other between the March 2011 calibration check and sol 100 indicating that the temperature dependence has stayed constant also in the absolute sense. We know that the temperature dependence of the Barocap® sensor heads has not drifted because the difference between pressure readings of any two sensor heads does not change with temperature, and based on test data, we know that it is unlikely that all four sensor heads would have exactly the same drift in their temperature dependence.

[27] REMS-P is not affected by the *thermal lag effect* that caused notable deviations in the data of the Phoenix pressure sensor [*Taylor et al.*, 2010]. In REMS compensation

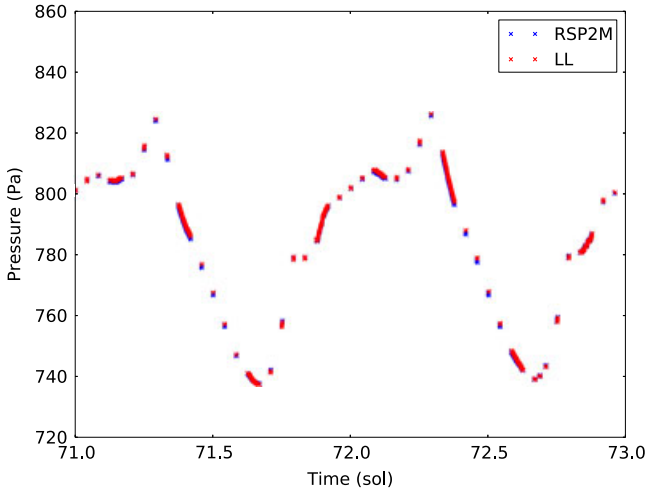

Figure 2. The diurnal pressure cycle over sols 71–74 with about 10% diurnal pressure variation, and showing also the pressure disturbances during the evening hours, most likely caused by local circulation phenomena.

for this effect is a part of the data processing pipeline. All housekeeping temperature data are downlinked, so unlike Phoenix, there are no residual errors caused by the interpolation of temperature data. Also, the temperature of the REMS-P changes with much slower rates than the temperature of the pressure sensors in Phoenix did.

[28] Before launch, it was considered a possibility that water outgassing of the pressure sensor head assemblies could cause deviations in the data measured during the first weeks after landing [*Gómez-Elvira et al.*, 2012]. However, the cruise phase calibrations showed that the water had outgassed fully prior to landing.

[29] We define the *absolute accuracy* of a single pressure reading as the greatest possible difference between the reading and true atmospheric pressure. Excluding data affected by the warm-up and shadow effects, the absolute accuracy is a sum of the maximum uncertainties that could be caused by the original calibration uncertainty, the effect of drift since the second cruise checkout, and the effect of repeatability variation. For the LL sensor head and before sol 100 the estimates of these are < 1.0 Pa, < 0.2 Pa, and < 1.5 Pa, respectively. Thus, the absolute accuracy of a single LL sensor head reading is estimated to be < 2.7 Pa during this time interval. The accuracy of a diurnal average is circa 0.5 Pa better than this because the diurnal repeatability variation averages out partly. Later in the mission the accuracy will slowly worsen as the uncertainty caused by the drift increases. When studying seasonal variation, drift is the only error source that needs to be taken into account (estimated to be circa 0.5 Pa/year for the LL sensor head). When studying diurnal-scale variations, the error source to be taken into account is the repeatability variation of ± 0.75 Pa.

3. First Analysis of Surface Pressure Observations

[30] The atmospheric pressure observations during the first 100 sols of MSL operations on the floor of Gale Crater have expanded our knowledge on the Martian atmosphere and have also revealed previously undetected phenomena. Sol by sol, the average atmospheric pressure is gradually increasing driven by the advancing northern summer and accompanying sublimation of the northern polar cap. However, the increase of the atmospheric pressure seems to be somewhat smaller than what has been observed by the earlier Martian missions indicating a possibility that the overall energy balance may be different for the current Martian year compared with those previous Martian years, of which earlier records of in situ observations are available. Then, the unique observational environment of the Gale Crater is creating regional, mesoscale and local circulation, and other atmospheric phenomena inside the Gale Crater and in the area covering the crater and its immediate surroundings. The pressure drops and small pressure oscillations revealed by MSL data may represent the local effects of Gale Crater (R. M. Haberle et al., Meteorological Predictions for the REMS Experiment on MSL, submitted to *Mars Journal*, 2012) and is an important issue for further detailed analysis.

[31] A first view on the atmospheric pressure is given by Figure 2 depicting hourly diurnal pressure over a period of the MSL sols 71–74. These sols present an example of a repeatable dust-free period. There are small changes in the sol-to-sol pressures primarily due to the progress of the season and other meteorological large-scale phenomena. The minimum and the maximum pressures increase over the duration of the plot by about 5 Pa. In overall, the diurnal variation in pressure, having the amplitude of about 90 Pa and caused mostly by the thermal tide, is similar from sol to sol. In the evening the increasing pressure trend is interrupted for 2–3 h, when the pressure briefly dips down between 5 and 10 Pa, before rising again, forming a shoulder-like feature at around midnight in the plot. The magnitude of this feature is clearly higher than the repeatability of REMS-P, and it is detected similarly by all sensor heads, indicating that it is not an instrument artifact. After continuing to rise for about 2 h, the trend reverses and the pressure begins a steep

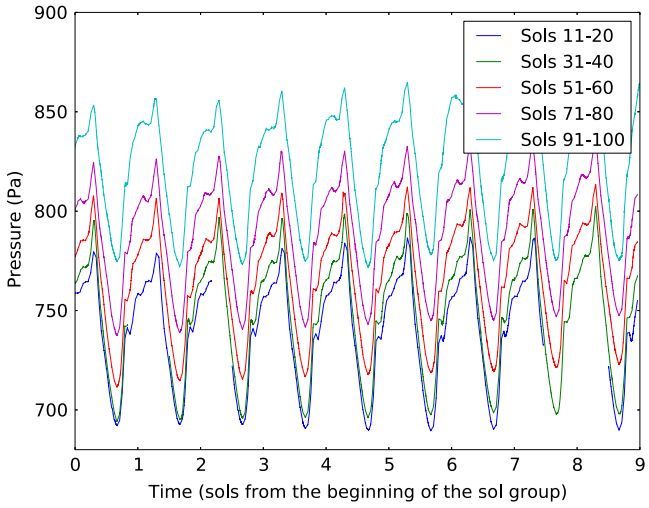

Figure 3. Diurnal pressure variation over the first 100 sols of MSL operations measured by the LL-type Barocap®. There are five groups of diurnal pressure cycles showing data from sols 11–20, 31–40, 51–60, 71–80, and 91–100. The gradually advancing season is evident through increasing pressure from group to group.

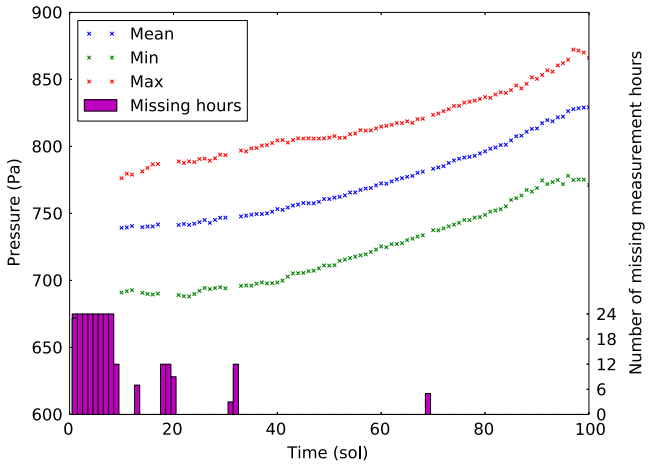

Figure 4. Diurnal maxima, means, and minima observed by REMS-P LL-type Barocap®. The bars at the bottom of the chart show the number of missing (hourly) observation sessions for each sol.

decline, forming a sharp peak at around 0600 LT. A minimum pressure is reached around 1600 LT before the pressure starts to rise again. MSL pressure observations show a sol-to-sol variation, including thermal tide signatures, as has been observed by previous in situ pressure measurements by Viking [*Soffen*, 1976], Pathfinder [*Schofield et al.*, 1997], and Phoenix missions [*Taylor et al.*, 2010]. The complex terrain surrounding MSL is likely causing local phenomena, e.g., katabatic winds over the rim of the Gale Crater which can be seen in our modeling results in Figure 11, contributing to a more complex structure seen in the pressure variations as was anticipated (R. M. Haberle et al., submitted manuscript, 2012).

[32] During the first 100 MSL sols, Curiosity has covered terrain having a maximal altitude difference of 17 m that corresponds to a pressure difference of about 1.2 Pa. This is a small number when assessing the seasonal variation of the surface pressure. However, the altitude could be taken into account and compensated for, when comparing sol-to-sol pressure variation at times when Curiosity has covered a significant distance.

[33] The advancing Martian season is apparent in the gradual pressure increase as shown in Figure 3, which groups together the daily variation in pressure. It shows clearly the repeatability of the sol-to-sol variability and the increase in pressure as the season advances from Northern summer into autumn.

[34] The mean of the pressure over 1 sol is a convenient way to demonstrate the sol by sol increasing atmospheric pressure. The pressure average, maximum and minimum values for the period of the first 100 MSL sols are shown in Figure 4. The mean of the pressure is calculated by first calculating the mean over a 5 min observational window, each hour, then taking the mean of the hourly means. This is done to prevent bias from the fact that there may be a significantly different number of measurements taken at different times of a sol. The first 180 s of each session are excluded when calculating the averages because of the warm-up effect. The mean of the pressure over a sol is increasing steadily, with the gradient increasing, while the difference between the maximum and minimum pressure is decreasing as the sols progress.

[35] The airborne dust affects the atmospheric pressure by increasing the heating of the atmosphere by absorbing incoming solar irradiation that then results in the cooling down of the surface. The amount of atmospheric dust can be estimated by optical thickness obtained by the MSL MastCam instrument [*Johnson et al.*, 2013]. The effect of dust afloat is illustrated in Figure 5 showing the atmospheric optical depth together with the diurnal variation (maximum-minimum) of atmospheric surface pressure. The optical thickness exhibits a decreasing trend during the MSL sols 30 to 90, after which it increases during the sols 90 to 100. There is a clear correlation between the airborne dust and variation of pressure such that pressure variation seems to be positively correlated with the airborne dustload. This is likely due to the fact that during the daytime airborne dust increases the heating of the atmosphere that will decrease the atmospheric surface pressure. The daytime pressure is decreasing with increased airborne dust, and hence, diurnal atmospheric pressure variation is increased with increasing airborne dustload, as shown by the data.

[36] When decomposing the pressure observations into a series representation through Fourier transformation, the estimated diurnal and semidiurnal amplitudes are revealed by the first and second harmonic components, respectively, as shown in Figure 6 together with the optical thickness observations by MastCam. The first and second harmonic illustrate the effect of airborne dust in a similar fashion as the diurnal pressure variation in the preceding figure by exhibiting a clear amplitude increase with the increasing amount of the atmospheric dust [*Zurek*, 1978, 1981, 1982; *Tillman*, 1988; *Kahre and Haberle*, 2010; *Rafkin*, 2009]. This illustrates how the Martian atmospheric conditions are intertwined with the airborne dust to such extent that atmospheric pressure observations could even be used to infer the amount of dust afloat. The data used for these plots are calculated using hourly averages for each sol. Only the sols that have exactly 24-hourly averages are shown.

[37] Some local atmospheric phenomena are visible in the first MSL pressure observations. For instance, Figure 7

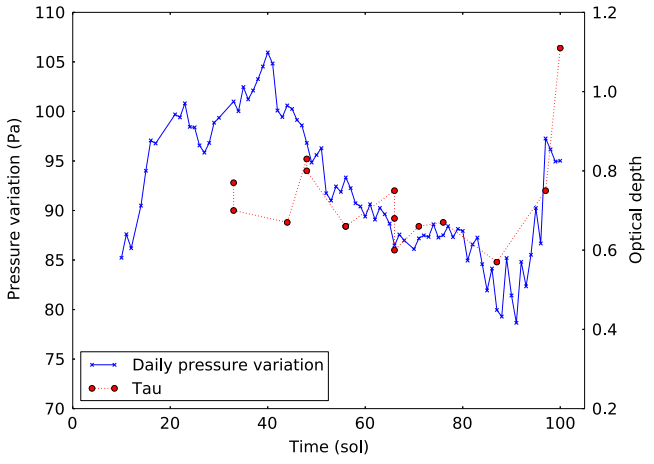

Figure 5. The effect of the atmospheric optical depth on the atmospheric pressure variation (difference between daily maximum and minimum pressure values).

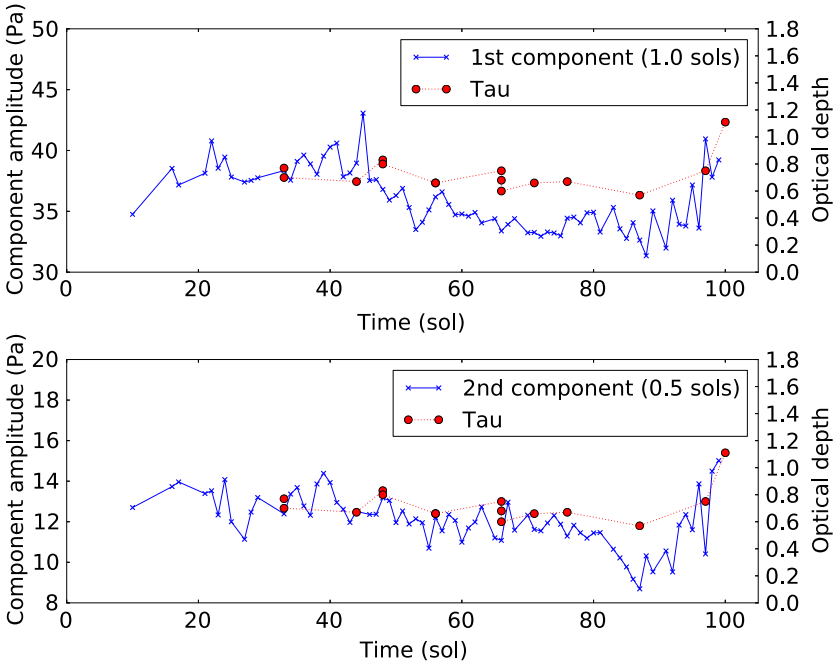

Figure 6. The atmospheric optical depth and the (top) 24 h pressure harmonic and (bottom) 12 h pressure harmonic. There is a positive correlation between the pressure harmonics and the atmospheric optical depth, clearly visible during the last 10 sols.

shows an example of a rapid warm-core pressure drop, most likely caused by a passage of a small thermal vortex such as a dust devil detected on the MSL sol 60. A sharp drop of about 1 Pa in pressure takes place around noon at 1218 LT. The first 100 sols of MSL pressure observations encompass a few similar kind of pressure drops that could be due to thermal vortices. Similar phenomena have been detected by, e.g., Pathfinder mission [*Ferri et al.*, 2003]. A statistical analysis of this phenomenon embedded in the MSL pressure and temperature data is under way.

[38] An unexpected phenomenon of rapid evening oscillations in the MSL surface pressure are highlighted in Figure 8 depicting the surface pressure at the local time period of 1900 LT–2130 LT on the MSL sol 48. This phenomenon has been detected more than once and it is occurring around the same local time. The amplitude of these oscillations is 0.25–0.5 Pa and their period appears to be 12–18 min. Detection of these oscillations requires that REMS is measuring continuously during a 1 or 2 h observation window during the

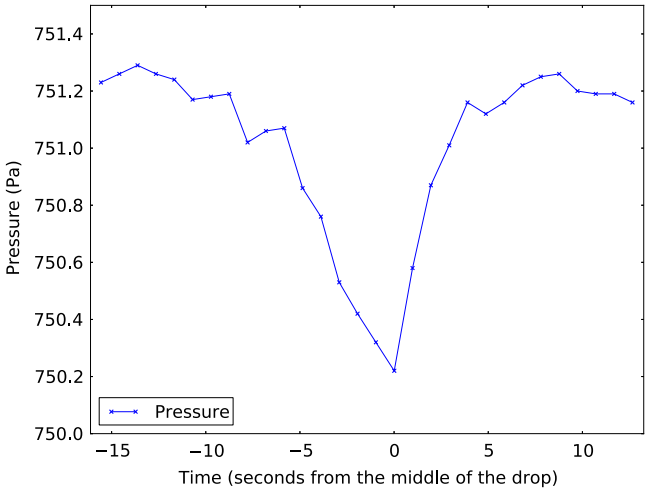

Figure 7. An example of a pressure drop (measured by RSP2M-type Barocap®), probably caused by a thermal vortex. This phenomenon takes place on the MSL sol 60 just after noon at about 1218 LT. There may also be a corresponding increase in atmospheric temperature, but this is still under evaluation. The abscissa is seconds, and the whole frame covers about 30 s.

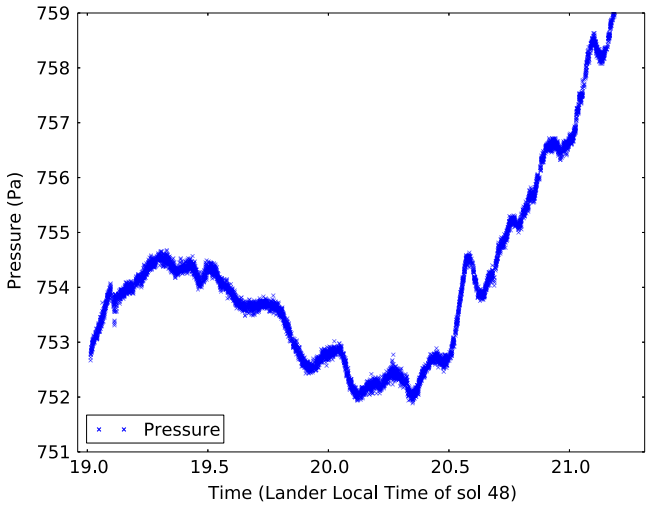

Figure 8. Pressure (RSP2M-type Barocap®) observations during local evening hours of 1900 LT to 2130 LT of sol 48. The observations exhibit oscillations that are likely caused by local circulation phenomena.

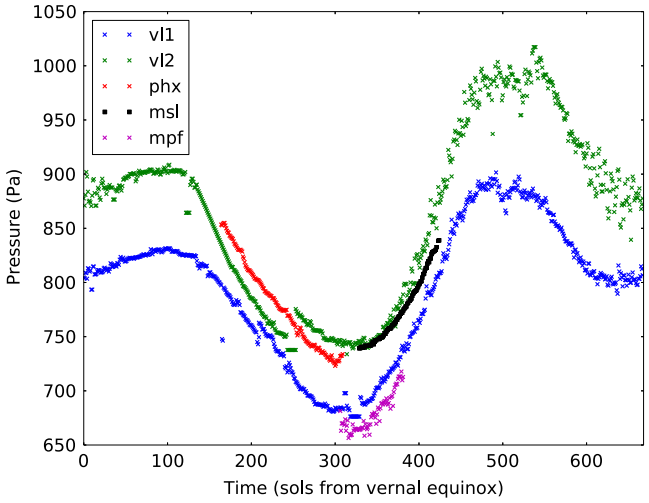

Figure 9. The sol-averaged surface pressure observed by earlier Mars landing missions and the MSL (black dots, LL-type Barocap®) as a function of sols starting from the vernal equinox.

evening hours. This actually took place only a few times during the first 100 MSL sols. As these oscillations tend to occur after sunset when the boundary layer has stabilized, they may be associated with gravity wave oscillations set up by the emerging drainage flows as seen in our modeling results in Figure 11 or perhaps emanating from above the boundary layer.

[39] As suggested by *Haberle et al.* [2014], this oscillation could be due to internal gravity waves excited by downslope flow. The apparent decay of these oscillations after 22:00 is plausibly due to wind shear driven near surface turbulence.

4. MSL Pressure Observations Combined With Modeling Results

[40] The MSL pressure observations are giving information on practically all the spatial and temporal scales of the Martian atmospheric phenomena ranging from micrometeorology to global atmospheric flows. To put the MSL pressure observations into a wider geographical and temporal context we have simulated the surface pressure and other atmospheric parameters by using a Global Circulation Model (GCM) by Ashima Research Inc. [*Richardson et al.*, 2007] and the Mars limited area model (MLAM) by the Finnish Meteorological Institute [*Kauhanen et al.*, 2008]. The simulated results seem to be in compliance with the actual observations and are shedding light on the environmental conditions of the surroundings outside the Gale Crater. Detailed modeling studies are needed to enhance our understanding on the Gale Crater environmental conditions.

[41] Figure 9 shows the sol-averaged surface pressure observed by MSL and earlier Mars landing missions as a function of the solar longitude. This helps us to place the MSL data in the correct context with regard to the evolution of the atmospheric pressure over the seasonal time scale, i.e., we expect the future pressure observations to show an increase and reach a maximum around the MSL sol 200. It also puts into context the time scales of the previous Mars landing missions compared to the MSL pressure data published in this paper. We already have data over similar time scales as the Pathfinder and Phoenix landers. When the MSL primary mission concludes within one Martian year from now, the accumulated data will approach the seasonal time scale of the Viking measurements.

[42] Figure 10 focuses on the period of the first 100 sols of REMS pressure measurements accompanied by the observations obtained from the other Mars landing missions. To compensate for the differences in elevation, an elevation correction based on a scale height of 11.0 km was used to transform all the pressures to the elevation of Viking Lander 1. Pathfinder pressure measurements are significantly lower than the observations by other missions, and the Phoenix pressure measurements show the highest pressure levels. On this scale, MSL pressure observations follow the VL1 and VL2 curves, but as we saw in Figure 9, there is a clear difference in growth speed. The fact that the seasonal increase of the surface pressure at Gale Crater seems to be taking place more slowly than what has been discovered by other landing missions calls for additional modeling investigations and data analysis.

[43] More detailed analysis is needed to really identify those phenomena that could be responsible for this observed slower than Viking rate of pressure rise. The relative difference between the MSL and Viking pressures, when adjusted for altitude could be due to topographical effects [*Haberle et al.*, 2014] and may even be an indication of secular climate change on Mars.

[44] The Mars limited area model (MLAM) is an adaptation of the high-resolution limited area model version 5.0 used for short-range weather prediction by the North European countries. Simulations at the Phoenix landing site are described by *Kauhanen et al.* [2008]. MLAM is a hydrostatic semi-Lagrangian semi-implicit model in a terrain-following hybrid vertical coordinate and latitude-longitude C-grid. The radiation scheme is from the University of Helsinki Mars 1-D model. The present simulations are

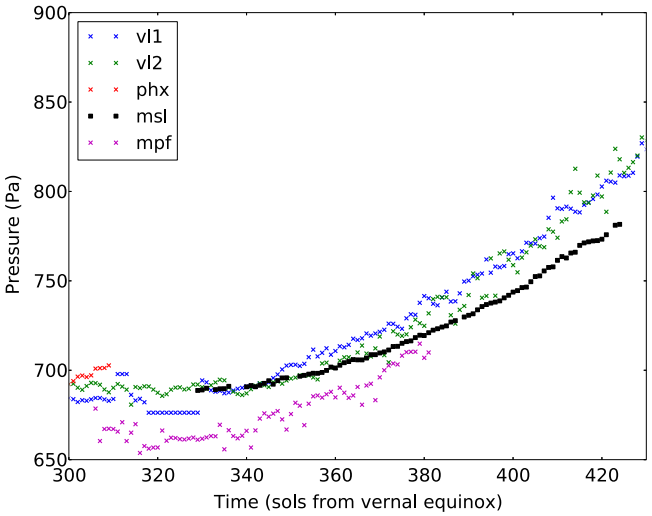

Figure 10. The sol-averaged surface pressure observed by MSL (black dots, LL-type Barocap®) and the earlier Mars landing missions. The pressures are adjusted for the elevation of VL1 to enable the comparison of the development of MSL pressure observations with the earlier missions.

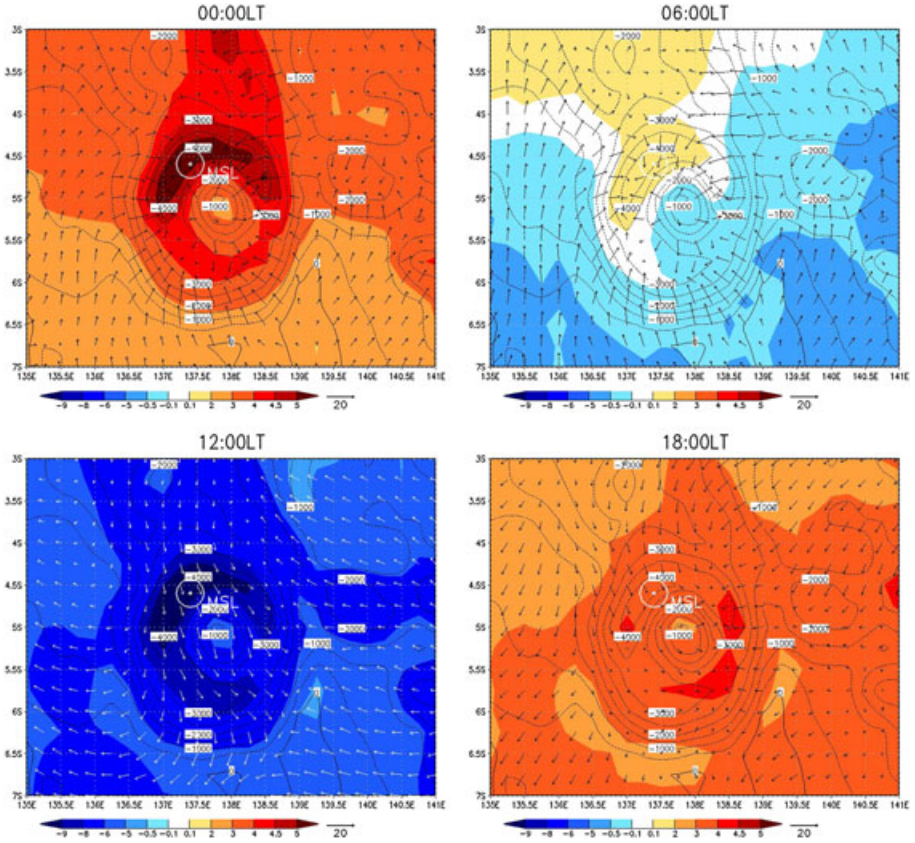

Figure 11. Surface geopotential (contours) and 30 sols mean of surface wind in meters per second (vectors) and hourly surface pressure tendency in pascals per hour (color bar) simulated by MLAM for 00, 06, 12, and 18 LT.

centred on Gale Crater, starting 5 sols before the scheduled MSL landing in nested grids of 1°, 0.5°, and 0.25° (60, 30, and 15 km) at 32 levels, the lowest levels being at about 1.7, 7, 32, and 75 m above the ground with the top at 47 km. The surface albedo, topography, and thermal inertia are based on Mars Global Surveyor (MGS) data, and the surface roughness is 1 cm. The initial boundary and dust fields are interpolated from the UKMGCM-assimilated (UK Mars Global Circulation Model) global 5° analyses of MGS/Thermal Emission Spectrometer observations from Mars Year 26, which is an average dust year.

[45] In Figure 11 sol 1–30 means of MLAM-hourly surface pressure tendencies and surface winds are depicted from the innermost 15 km grid spacing simulation. The area of each plot in the figure corresponds to around 80,000 km^2. MLAM reproduces the diurnal pressure variation as shown in the observations with increasing pressure everywhere at midnight, most steeply around the MSL landing site, decreasing pressure in the morning at 0600, decreasing pressure at noon, and increasing pressure in the evening at 1800.

[46] The repeatable shape of the diurnal surface pressure profile and its strong diurnal variation (Figures 2 and 3) is probably mostly due to the strong diurnal thermal tide effect on Mars, as e.g., in Pathfinder [*Schofield et al.*, 1997]. However, local modifications may exist due to the more complex topography as compared to the flat and smooth Pathfinder site. Again, a more comprehensive study is needed, but our prelanding local forecasts for the MSL site made with the Mars limited area model (MLAM) do suggest local pressure tendency effects, described below, which are associated with local slope winds.

[47] The 30 sols means of MLAM-hourly surface pressure tendencies and surface winds are depicted in Figure 11 for 00 LT and 12 LT from the 15 km grid simulation. MLAM underestimates the surface pressures at the MSL site by about 5 % (due to the boundary conditions) but simulates the strong diurnal variation caused by the global thermal tide quite well. Interestingly, Figure 11 also suggests local dynamical effects: The 00 LT general surface pressure rise is strongest at the Gale Crater floor, where local drainage flows down the cold steep slopes of the crater rim and Mount Sharp are seen to converge strongly. This may increase the surface pressures [*Haberle et al.*, 2014]. The rapid pressure that falls at 12 LT are likewise strong at the crater floor, where local flows up the sun-warmed slopes diverge, embedded on winds due to larger-scale upslope, tidal and trade wind origin.

5. Discussion

[48] REMS-P, the pressure measurement subsystem of the MSL Rover Environmental Monitoring Station (REMS) has completed its first 100 sols of observations on the Martian surface in the Gale Crater. These observations are the first in

situ pressure measurements in the Martian equatorial regions and the first performed on a mobile surface platform.

[49] The REMS-P has performed according to expectations with high data quality and good coverage. After the commissioning phase taking place on the MSL mission sols 2–8, REMS-P has successfully created a record of hourly pressure observations with gaps only during the hours of REMS instrument inspections or MSL level system checks.

[50] The REMS-P observations during the first 100 MSL sols have witnessed atmospheric features at various spatial and temporal scales, e.g., the gradually increasing pressure due to the advancing Martian season, diurnal tides, thermal vortices, and other local atmospheric phenomena. The surface pressure data has also revealed previously unobserved phenomena, e.g., a small regular pressure drop at about 20 LT every sol, and small pressure oscillations occurring in the early evening. Overall, the effect of the complex terrain around the Gale Crater may have a role with these phenomena.

[51] A distinct coupling between the atmospheric dust load and the pressure signal is also evident in the pressure observations in spite of the available atmospheric dust observations (column optical thickness) being sparse. The correlation between surface pressure and dust opacity was first detected by Viking landers. The MSL pressure observations have been preliminarily compared with regional model results, and the agreement between observations and models appears to be good.

[52] We are looking forward to continued high-quality observations by the REMS-P, extending the data set to reveal seasonal variations. The Martian atmosphere will go through the peak seasonal pressure approximately during the next 150 sols, which is a highly interesting event in the near future. Increased amount of data will also allow improved insights into regional and local phenomena and their seasonal dependencies. The effects of the changing location of the MSL rover may also become visible later in the mission, when the displacement between the measurement location and the landing site increases.

[53] **Acknowledgments.** The authors would like to express their gratitude to the MSL and REMS instrument teams in making this wonderful Mars mission come true. Ari-Matti Harri and Hannu Savijarvi are thankful for the Finnish Academy grants 132825 and 131723.

References

Barnes, J. R., J. B. Pollack, R. M. Haberle, C. B. Leovy, R. W. Zurek, H. Lee, and J. Schaeffer (1993), Mars atmospheric dynamics as simulated by the NASA Ames general circulation model: 2. Transient baroclinic eddies, *J. Geophys. Res.*, *98*, 3125–3148.

Ellehoj, M. D., et al. (2010), Convective vortices and dust devils at the Phoenix Mars mission landing site, *J. Geophys. Res.*, *115*, E00E16, doi:10.1029/2009JE003413.

Ferri, F., P. H. Smith, M. Lemmon, and N. O. Rennó (2003), Dust devils as observed by Mars Pathfinder, *J. Geophys. Res.*, *108*(E12), 5133, doi:10.1029/2000JE001421.

Forget, F., F. Hourdin, R. Fournier, C. Hourdin, O. Talagrand, M. Collins, S. R. Lewis, P. L. Read, and J.-P. Huot (1999), Improved general circulation models of the Martian atmosphere from the surface to above 80 km, *J. Geophys. Res.*, *104*, 24,155–24,176, doi:10.1029/1999JE001025.

Gómez-Elvira, J., et al. (2012), REMS: The environmental sensor suite for the Mars Science Laboratory rover, *Space Sci. Rev.*, *170*, 583–640, doi:10.1007/s11214-012-9921-1.

Haberle, R. M., H. C. Houben, R. Hertenstein, and T. Herdtle (1993), A boundary-layer model for Mars: Comparison with Viking lander and entry data, *J. Atmos. Sci.*, *50*, 1544–1559, doi:10.1175/1520-0469(1993)050<1544:ABLMFM>2.0.CO;2.

Haberle, R. M., J. B. Pollack, J. R. Barnes, R. W. Zurek, C. B. Leovy, J. R. Murphy, H. Lee, and J. Schaeffer (1993), Mars atmospheric dynamics as simulated by the NASA Ames general circulation model: 1. The zonal-mean circulation, *J. Geophys. Res.*, *98*, 3093–3124.

Haberle, R. M., et al. (2014), Preliminary interpretation of the REMS pressure data from the first 100 sols of the MSL mission, *J. Geophys. Res. Planets*, doi:10.1002/2013JE004488.

Harri, A.-M., et al. (1998), Meteorological observations on Martian surface: Met-packages of Mars-96 Small Stations and Penetrators, *Planet. Space Sci.*, *46*, 779–793, doi:10.1016/S0032-0633(98)00012-9.

Harri, A.-M., T. Mäkinen, A. Lehto, H. Kahanpää, and T. Siili (2006), Vertical pressure profile of Titan—Observations of the PPI/HASI instrument, *Planet. Space Sci.*, *54*, 1117–1123, doi:10.1016/j.pss.2006.05.037.

Hess, S. L., R. M. Henry, C. B. Leovy, J. A. Ryan, and J. E. Tillman (1977), Meteorological results from the surface of Mars: Viking 1 and 2, *J. Geophys. Res.*, *82*, 4559–4574, doi:10.1029/JS082i028p04559.

James, P. B., H. H. Kieffer, and D. A. Paige (1992), The seasonal cycle of carbon dioxide on Mars, in *Mars*, edited by H. H. Kieffer et al., pp. 934–968, Univ. of Ariz. Press, Tucson, Ariz.

Johnson, J. R., J. F. Bell, A. G. Hayes, R. Deen, A. Godber, J. Joseph, R. E. Arvidson, M. Lemmon, and MSL Science Team (2013), Preliminary Mastcam visible/near-infrared spectrophotometric observations at the curiosity landing site, Mars, *Proc. Lunar Planet. Sci. Conf. 44th*, *LPI Contributions*, *1719*, 1374 pp., Woodlands, Tex.

Kahre, M. A., and R. M. Haberle (2010), Mars CO_2 cycle: Effects of airborne dust and polar cap ice emissivity, *Icarus*, *207*, 648–653.

Kauhanen, J., T. Siili, S. Järvenoja, and H. Savijärvi (2008), The Mars limited area model and simulations of atmospheric circulations for the Phoenix landing area and season of operation, *J. Geophys. Res.*, *113*, E00A14, doi:10.1029/2007JE003011.

Kliore, A., D. L. Cain, G. S. Levy, V. R. Eshleman, G. Fjeldbo, and F. D. Drake (1965), Occultation experiment: Results of the first direct measurement of Mars's atmosphere and ionosphere, *Science*, *149*(3689), 1243–1248, doi:10.1126/science.149.3689.1243.

Leovy, C. B., and Y. Mintz (1969), Numerical simulation of the atmospheric circulation and climate of Mars, *J. Geophys. Res.*, *26*, 1167–1190.

Martin, L. J., P. B. James, A. Dollfus, K. Iwasaki, and J. D. Beish (1992), Telescopic observations: Visual, photographic, polarimetric, in *Mars*, edited by H. H. Kieffer et al., pp. 34–70, Univ. of Ariz. Press, Tucson, Ariz.

Paige, D. A., W. V. Boynton, D. Crisp, E. DeJong, A. M. Harri, C. J. Hansen, H. U. Keller, L. A. Leshin, P. H. Smith, and R. W. Zurek (1998), Mars Volatiles and Climate Surveyor (MVACS) integrated payload for the Mars Polar Lander mission, paper presented at 1st International Conference on Mars Polar Science and Exploration, *LPI Contributions*, *953*, 30 pp., Lunar and Planet. Inst., Houston, Tex.

Petrosyan, A., et al. (2011), The Martian atmospheric boundary layer, *Rev. Geophys.*, *49*, RG3005, doi:10.1029/2010RG000351.

Pollack, J. B., R. M. Haberle, J. Schaeffer, and H. Lee (1990), Simulations of the general circulation of the Martian atmosphere: 1. Polar processes, *J. Geophys. Res.*, *95*, 1447–1473.

Pollack, J. B., R. M. Haberle, J. R. Murphy, J. Schaeffer, and H. Lee (1993), Simulations of the general circulation of the Martian atmosphere: 2. Seasonal pressure variations, *J. Geophys. Res.*, *98*, 3149–3182.

Rafkin, S. C. R. (2009), A positive radiative-dynamic feedback mechanism for the maintenance and growth of Martian dust storms, *J. Geophys. Res.*, *114*, E01009, doi:10.1029/2008JE003217.

Rafkin, S. C. R., R. M. Haberle, and T. I. Michaels (2001), The Mars Regional Atmospheric Modeling System: Model description and selected simulations, *Icarus*, *151*, 228–256, doi:10.1006/icar.2001.6605.

Richardson, M. I., A. D. Toigo, and C. E. Newman (2007), PlanetWRF: A general purpose, local to global numerical model for planetary atmospheric and climate dynamics, *J. Geophys. Res.*, *112*, E09001, doi:10.1029/2006JE002825.

Schofield, J. T., J. R. Barnes, D. Crisp, R. M. Haberle, S. Larsen, J. A. Magalhaes, J. R. Murphy, A. Seiff, and G. Wilson (1997), The Mars Pathfinder Atmospheric Structure Investigation/Meteorology (ASI/MET) experiment, *Science*, *278*, 1752–1758, doi:10.1126/science.278.5344.1752.

Seiff, A., et al. (1997), The atmosphere structure and meteorology instrument on the Mars Pathfinder lander, *J. Geophys. Res.*, *102*, 4045–4056, doi:10.1029/96JE03320.

Snyder, C. W., and V. I. Moroz (1992), Spacecraft exploration of Mars, in *Mars*, edited by H. H. Kieffer et al., chap. 2, pp. 71–119, Univ. of Ariz. Press, Tucson, Ariz.

Soffen, G. A. (1976), Scientific results of the Viking missions, *Science*, *194*, 1274–1276, doi:10.1126/science.194.4271.1274.

Spiga, A. (2011), Elements of comparison between Martian and terrestrial mesoscale meteorological phenomena: Katabatic winds and boundary layer convection, *Planet. Space Sci.*, *59*, 915–922.

Taylor, P. A., D. C. Catling, M. Daly, C. S. Dickinson, H. P. Gunnlaugsson, A.-M. Harri, and C. F. Lange (2008), Temperature, pressure, and wind instrumentation in the Phoenix meteorological package, *J. Geophys. Res.*, *113*, E00A10, doi:10.1029/2007JE003015.

Taylor, P. A., et al. (2010), On pressure measurement and seasonal pressure variations during the Phoenix mission, *J. Geophys. Res.*, *115*, E00E15, doi:10.1029/2009JE003422.

Tillman, J. E. (1988), Mars global atmospheric oscillations: Annually synchronized, transient normal-mode oscillations and the triggering of global dust storms, *J. Geophys. Res.*, *93*, 9433–9451, doi:10.1029/JD093iD08p09433.

Tillman, J. E., R. M. Henry, and S. L. Hess (1979), Frontal systems during passage of the Martian north polar hood over the Viking Lander 2 site prior to the first 1977 dust storm, *J. Geophys. Res.*, *84*, 2947–2955, doi:10.1029/JB084iB06p02947.

Towner, M. C., et al. (2004), The Beagle 2 environmental sensors: Science goals and instrument description, *Planet. Space Sci.*, *52*, 1141–1156.

Wray, J. J. (2013), Gale Crater: The Mars Science Laboratory/Curiosity Rover Landing Site, *Int. J. Astrobiol.*, *12*, 25–38, doi:10.1017/S1473550412000328.

Zurek, R. W. (1978), Solar heating of the Martian dusty atmosphere, *Icarus*, *35*, 196–208, doi:10.1016/0019-1035(78)90005-2.

Zurek, R. W. (1981), Inference of dust opacities for the 1977 Martian great dust storms from Viking Lander 1 pressure data, *Icarus*, *45*, 202–215, doi:10.1016/0019-1035(81)90014-2.

Zurek, R. W. (1982), Martian great dust storms: An update, *Icarus*, *50*, 288–310, doi:10.1016/0019-1035(82)90127-0.

Zurek, R. W. (1992), Comparative aspects of the climate of Mars: An introduction to the current atmosphere, in *Mars*, edited by H. H. Kieffer et al., pp. 799–817, Univ. of Ariz. Press, Tucson, Ariz.

Zurek, R. W., J. R. Barnes, R. M. Haberle, J. B. Pollack, J. E. Tillman, and C. B. Leovy (1992), Dynamics of the atmosphere of Mars, in *Mars*, edited by H. H. Kieffer et al., pp. 835–934, Univ. of Ariz. Press, Tucson, Ariz.